Available online at www.sciencedirect.com
SCIENCE DIRECT®
Physica E 20 (2004) 268–271
PHYSICA E
www.elsevier.com/locate/physe

Microscopic modeling of intersubband resonances in InAs/AlSb quantum wells

J. Li[a,*], K.I. Kolokolov[a], C.Z. Ning[a], D.C. Larrabee[b], G.A. Khodaparast[b], J. Kono[b], K. Ueda[c], Y. Nakajima[c], S. Sasa[c], M. Inoue[c]

[a] *Center for Nanotechnology, M/S N229-1, NASA Ames Research Center, Moffett Field, CA 94035, USA*
[b] *Department of Electrical and Computer Engineering, Rice University, Houston, TX 77005, USA*
[c] *Department of Electrical Engineering, Osaka Institute of Technology, Osaka, Japan*

Abstract

Linear absorption spectra from intersubband resonance in InAs/AlSb quantum wells are analyzed theoretically using the intersubband semiconductor Bloch equation approach. Our model goes beyond the Hartree–Fock approximation and treats particle–particle correlations under the second Born approximation. Electron–electron and longitudinal optical phonon scatterings from such a treatment describe intrinsic line broadening to the intersubband resonance. Electron subbands are determined self-consistently with a spurious-state-free 8-band $\boldsymbol{k}\cdot\boldsymbol{p}$ Hamiltonian under the envelope function approximation. To compare with experimental measurements, we also included line broadening due to electron-interface roughness scattering. Excellent agreement was achieved for temperature-dependent absorption spectra in the mid-infrared frequency range, after taking into careful account the interplay of material parameters, nonparabolicity in bandstructure, and many-body effects.

PACS: 78.67.De; 78.30.Fs; 78.20.Bh; 73.21.Fg

Keywords: Intersubband resonance; Quantum wells; InAs/AlSb; Many-body effects

1. Introduction

Compact and efficient infrared (IR) light sources are needed for portable and small footprint sensing and communications. In particular, far infrared (FIR) coherent sources of this type are useful to identify molecular species and imaging. One way to generate coherent IR radiation is using intersubband resonance (ISBR) in quantum well (QW) structures [1]. Owing to quantum confinement effect, subbands are formed and intersubband transitions are possible by electric dipole coupling to the light field. Naturally, light absorption and photoluminescence serve as excellent spectroscopic mechanisms for characterization and investigation of the devices.

In our effort to generate FIR radiation, we have chosen an Sb-based compound semiconductor heterostructure, or InAs/AlSb quantum wells. For this study on sample characterization and physical model validation we chose 10 nm thick QWs, which have about 200 meV (mid-IR) intersubband separation. The 20 periods of QWs were grown by molecular beam epitaxial (MBE) and details are given separately in Ref. [2]. The samples were unintentionally doped

* Corresponding author. Tel.: +1-650-604-4410; fax: +1-650-604-0987.
E-mail address: jianzhng@nas.nasa.gov (J. Li).

1386-9477/$ - see front matter © 2003 Elsevier B.V. All rights reserved.
doi:10.1016/j.physe.2003.08.016

and electron density was determined by Hall and Shubnikov–de Haas measurements to be in the range of 1–10 $\times$ 10^{11} cm^{-2} per well. ISBR spectra were obtained by Fourier-transform infrared spectroscopy in a wave guide geometry as a function of temperature (T). Theoretically, the Hartree–Fock approach based on density matrix theory was used to account for many-body effects, including self-energy, vertex contribution, depolarization field, and dephasing (leading to line broadening) due to electron–electron and longitudinal optical (LO) phonon scatterings [3,4]. The thus derived intersubband polarization (induced by light field) equation was numerically solved by matrix inversion. As input for numerical analysis of the equation, subband dispersions were calculated self-consistently for single QW case by assuming uniformly distributed (2 nm thick) and fully ionized dopants in the neighboring barrier region [7]. Microscopic aspects of the equation are given in the next section, followed by illustration of the interplay of material parameters, nonparabolicity in bandstructure, and many-body effects, and comparison of the simulation results with typical ISBR spectra in Section 3. The achieved agreement in all-around characteristics between simulated ISBR spectra and experiments validates our microscopic model. We conclude with a summary in Section 4.

2. Theoretical approach

We modeled the experiments from a single QW viewpoint. The experimental samples had 20 periods of QWs, but electrons in different wells were treated independently because of strong confinement. Inhomogeneous line broadening due to well-to-well fluctuation was ignored. The physical system consists of an interacting electron gas confined within a QW, which is subject to scatterings by interface roughness (IFR), LO phonons, and electrons themselves, resulting in line broadening for ISBRs. We adopted a perturbative approach to treatment of the Coulomb interaction among electrons and electron–LO phonon (Fröhlich) interaction in the framework of Hartree–Fock approach [4]. We ignored light propagation effect.

We derived the equation of motion (EOM) for dynamic variable $f_{mn}(\boldsymbol{k})$, where m, n label ground (=1) and excited subband (=2), and $\boldsymbol{k}$ is the in-plane wave vector (perpendicular to $\hat{\boldsymbol{z}}$ direction). Specifically, $f_{11}(\boldsymbol{k})$ ($f_{22}(\boldsymbol{k})$) is electron distribution function for the ground (excited) subband. $p(\boldsymbol{k}) \equiv f_{12}(\boldsymbol{k})$ is the intersubband polarization function. The resultant EOMs are termed the intersubband semiconductor Bloch equations. In linear absorption regime which this study covered, the electron distributions were given by Fermi function, whereas the intersubband polarization equation was linearized with respect to the light field. The rotating wave approximation was invoked and an ansatz $p(\boldsymbol{k}) = P_{\boldsymbol{k}}\exp(-\mathrm{i}\omega t)$ for the incident light field $\boldsymbol{E}_{\perp}(t) = E_0\exp(-\mathrm{i}\omega t)\hat{\boldsymbol{z}}$ was made. Then the intersubband polarization equation was reduced to

$$\{\hbar[\omega + \mathrm{i}\gamma_p(\boldsymbol{k})] - (\varepsilon_{2\boldsymbol{k}} - \varepsilon_{1\boldsymbol{k}})\}P_{\boldsymbol{k}} + \mathrm{i}\hbar\,\mathrm{d}P_{\boldsymbol{k}}/\mathrm{d}t|_{\mathrm{inc}}^{(\mathrm{nd})} = (d_{\boldsymbol{k}}E_0 - \varepsilon_{21\boldsymbol{k}})(f_{22\boldsymbol{k}} - f_{11\boldsymbol{k}}), \quad (1)$$

where $\gamma_p(\boldsymbol{k})$ includes all the diagonal parts of scatterings. The *n*on-*d*iagonal contributions from electron–LO phonon and –electron scatterings are given by the term with superscript (nd), whereas its subscript inc denotes the incoherent nature of scatterings. $\varepsilon_{m\boldsymbol{k}} = E_m(\boldsymbol{k}) + \varepsilon_{mm\boldsymbol{k}}$ consists of subband energy dispersion (first term) and self-energy (second term). $d_{\boldsymbol{k}}$ is the electric dipole matrix element for TM light field. $\varepsilon_{21\boldsymbol{k}}$ gives rise to the local field effect, which has two sources: a vertex correction that reflects the nonlocal nature of exchange interaction, and a depolarization field term that arises from dynamic screening due to direct Coulomb interaction among electrons. (Refer to [5] for details.) Numerical matrix inversion was performed to obtain $P_{\boldsymbol{k}}$. Then the optical susceptibility was given by $\chi(\omega) \equiv P/\varepsilon_0 E_0$ where the total polarization $P = 2S/[(2\pi)^2\mathscr{V}]\int \mathrm{d}\boldsymbol{k}\,\mathrm{d}_{\boldsymbol{k}}^{*}P_{\boldsymbol{k}}$. $\mathscr{V} = WS$, W is the QW thickness and S is a normalization area. The absorbance is given by $2W\alpha(\omega)$ (per bounce at full TM polarization), where the absorption coefficient $\alpha(\omega) \approx \omega\,\mathscr{I}\mathrm{m}[\chi(\omega)]/nc$. n is the background refractive index and c is the speed of light in vacuo.

As input to Eq. (1), energy dispersion $E_m(\boldsymbol{k})$ was obtained self-consistently from a spurious-state-free 8-band $\boldsymbol{k}\cdot\boldsymbol{p}$ model [6] under the envelope function approximation [7]. Dephasing from IFR scattering was evaluated with Ando's theory [8], whereas other contributions were treated within the second Born approximation [3,4]. The single plasmon pole

approximation was used for screening electron–LO phonon and –electron interactions [3], whereas screening by phonons was neglected (in mid-IR frequency range). Modeling details will be published elsewhere [9].

3. Comparison with experiments

There were two outstanding material issues in modeling ISBRs. First, T-dependence of subband energy dispersions and electron density is needed. To this end, parameters in the $\boldsymbol{k}\cdot\boldsymbol{p}$ model were adjusted to reproduce the measured T-dependence of the InAs conduction band effective mass. Also, a T-dependent contribution was added to an MBE-operation-dependent constant base density: $n = N_{\mathrm{d}} + n_{\mathrm{CH}}(T)$. This extra portion is rather universal in InAs/AlSb QWs [10] and we call it Chadi term [11]. We modified Chadi's treatment by an adjusting prefactor (α):

$$n_{\mathrm{CH}}(T) = \alpha * D_{\mathrm{2D}} \frac{AT^2}{T+\beta}, \tag{2}$$

where α was taken to be $\frac{1}{3}$ to put the density increase from 0 to 300 K in the experimental value range of 2–3 $\times 10^{11}$ cm^{-2} [10], D_{2D} is the 2D electron density of states, and the fraction gives the T-dependent part of the InAs band gap. The values for these parameters were taken from Chadi's work [11]. Second, IFR dephasing is the leading line broadening mechanism in GaAs QWs [12]. Here we showed for InAs QWs that even though IFR plays a significant role at low T, dephasing by LO phonon and electron scatterings becomes predominant at high T and density level, partly owing to large nonparabolicity in InAs [9]. Since the IFR parameters, i.e., fluctuation height Δ and coherence length Λ, are unknown, we fixed Δ to be 4 Å and treated Λ as an adjustable one with a default value of 43 Å [12].

With these caveats we now discuss modeling of ISBR spectra of 10 nm InAs/AlSb QWs (Fig. 1). Experimental spectra were plotted as $-t\log r/w$ (t: wave guide thickness; w: width; r: ratio of s/p polarization transmission ratio *with* QWs over the transmission ratio *without* QWs). This expression differs from the fully-TM-polarized single-bounce absorbance by a constant, $N\sin(2\theta)/4\ln 10$ (N: QW periods; θ: angle of incidence). For absolute comparison the theoretical

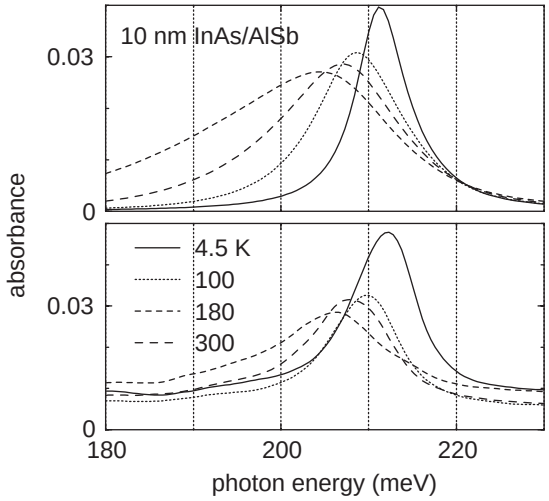

Fig. 1. Quantitative comparison of theoretical (upper) and experimental (lower) absorbance. Parameter values used in simulation: base electron density $N_{\mathrm{d}} = 2 \times 10^{11}$ cm^{-2}, interface fluctuation height $\Delta = 4$ Å, and coherence length $\Lambda = 51$ Å.

spectra were multiplied by this constant. Absorbance is roughly proportional to electron density, which allowed us to gauge the base density used in our simulation. However, to specify the base density N_{d} and IFR parameter Λ we first investigated their effects, as shown in Fig. 2. With one exception (explained below), the left column shows ISBR spectra with default IFR dephasing, whereas the right column depicts the spectra with the default IFR dephasing doubled. Same density was used in the same row. Doubling IFR dephasing broadens the ISBR line shape; the effect is enhanced at low T when dephasing caused by LO phonon and electron scatterings is impeded due to phase-space filling effect for electrons and reduction in phonon population. The relative ISBR strength at different temperature is thus modified, as a function of N_{d} and subject to the influence of the Chadi term. It is easy to see that at high T scatterings by LO phonons and electrons dominate over IFR effect. This investigation enabled us to estimate N_{d} from high T ISBRs and IFR dephasing from low T spectra. (This explains the exception in Fig. 2, which was a result of the recursive process that allowed us to obtain $\Lambda = 51$ Å $\approx$ 43 Å $\times \sqrt{1.4}$ in Fig. 1. Note that the IFR dephasing rate is proportional to $\Delta^2\Lambda^2$ and independent of temperature.) The set of parameters thus determined led to

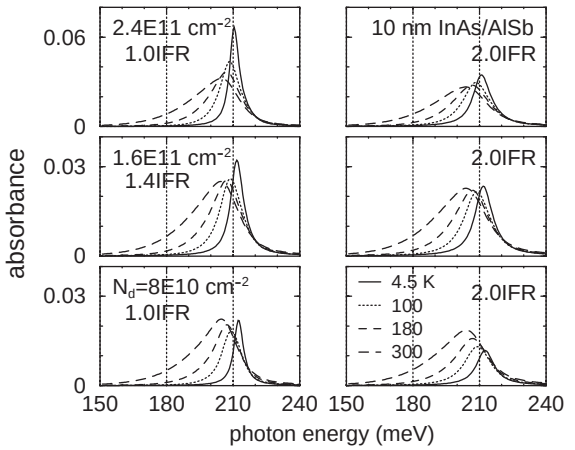

Fig. 2. Effects of adjusting IFR dephasing and T-dependence of electron density via Chadi term. Base electron densities (N_d) are the same in the same row. IFR dephasing rate was doubled in the right column from default values (corresponding to $\Delta = 4$ Å and $\Lambda = 43$ Å) in the left column (except mid-panel—1.4 times the default dephasing rate).

an excellent overall agreement between the simulated spectra and the experimental ones (Fig. 1), in terms of line shape, width, peak position, and its T-dependence.

Finally, we note that the above comparison is quantitative and absolute with all relevant parameters either given independently or determined within acceptable range. Furthermore, optimization permitted, our theoretical modeling promises an independent approach to determination of such hard-to-measured quantities, such as IFR coherence length.

4. Summary

To summarize, we presented our comprehensive theoretical effort to modeling InAs/AlSb quantum-well intersubband resonances and demonstrated excellent agreement with experiments. The intersubband semiconductor Bloch equations were derived by Hartree–Fock approach. Linear absorption from intersubband resonance was evaluated by numerically solving the polarization equation. Proper consideration was given to all major physical effects, such as nonparabolicity and self-consistency in bandstructure, temperature dependence of material parameters, and many-body effects. Thanks to all the extra efforts, the satisfactory results not only serve our characterization purpose, validate our theoretical model, but also suggest a new way of measurement of electron density and quantification of interface roughness.

Acknowledgements

This work is supported by a DARPA–AFOSR grant and by a joint NASA–NCI program.

References

[1] H.C. Liu, F. Capasso (Eds.), Intersubband Transitions in Quantum Wells: Physics and Device Application I, Academic Press, San Diego, CA, 2000.
[2] D.C. Larrabee, G.A. Khodaparast, J. Kono, K. Ueda, Y. Nakajima, M. Nakai, S. Sasa, M. Inoue, K.I. Kolokolov, J. Li, C.Z. Ning, Appl. Phys. Lett., accepted for publication.
[3] H. Haug, S.W. Koch, Theory of the Electrical and Optical Properties of Semiconductors, World Scientific, Singapore, 1992;
W.W. Chow, S.W. Koch, Semiconductor-Laser Fundamentals: Physics of the Gain Materials, Springer, Berlin, 1999.
[4] T. Kuhn, in: E. Schöll (Ed.), Theory of Transport Properties of Semiconductor Nanostructures, Chapman & Hall, London, 1998, p. 173.
[5] J. Li, C.Z. Ning, Phys. Rev. Lett. 91 (2003) 097401.
[6] K.I. Kolokolov, J. Li, C.Z. Ning, Phys. Rev. B 68 (2003) 161308 (R).
[7] J. Li, K. Kolokolov, C.Z. Ning, D.C. Larrabee, G.A. Khodaparast, J. Kono, K. Ueda, Y. Nakajima, S. Sasa, M. Inoue, MRS Proc. 744 (2003) 571.
[8] T. Ando, Z. Phys. B 24 (1976) 33;
T. Ando, J. Phys. Soc. Japan 54 (1985) 2671.
[9] J. Li, K.I. Kolokolov, C.Z. Ning, D.C. Larrabee, G.A. Khodaparast, J. Kono, K. Ueda, Y. Nakajima, S. Sasa, M. Inoue, unpublished.
[10] C. Nguyen, B. Brar, H. Kroemer, J. English, J. Vac. Sci. Technol. B 10 (1992) 898;
H. Kroemer, C. Nguyen, B. Brar, J. Vas. Sci. Technol. B 10 (1992) 1769;
S. Ideshita, A. Furukawa, Y. Mochizuki, M. Mizuta, Appl. Phys. Lett. 60 (1992) 2549.
[11] D.J. Chadi, Phys. Rev. B 47 (1993) 13478.
[12] T. Unuma, M. Yoshita, T. Noda, H. Sakaki, H. Akiyama, J. Appl. Phys. 93 (2003) 1586;
T. Unuma, T. Takahashi, T. Noda, M. Yoshita, H. Sakaki, M. Baba, H. Akiyama, Appl. Phys. Lett. 78 (2001) 3448;
J.B. Williams, M.S. Sherwin, K.D. Maranowski, A.C. Gossard, Phys. Rev. Lett. 87 (2001) 037401;
C.A. Ullrich, G. Vignale, Phys. Rev. Lett. 87 (2001) 037402.